

Article

Absolute Absorption Cross Section of the $\tilde{A} \leftarrow \tilde{X}$ Electronic Transition of the Ethyl Peroxy Radical and Rate Constant of its Cross Reaction with HO₂

Cuihong Zhang^{1,2,3}, Mirna Shamas¹, Mohamed Assali¹, Xiaofeng Tang^{2,3}, Weijun Zhang^{2,3}, Laure Pillier¹, Coralie Schoemaeker¹ and Christa Fittschen^{1,*}

¹ Université Lille, CNRS, UMR 8522 - PC2A - Physicochimie des Processus de Combustion et de l'Atmosphère, F-59000 Lille, France

² Laboratory of Atmospheric Physico-Chemistry, Anhui Institute of Optics and Fine Mechanics, Chinese Academy of Sciences, Hefei 230031, Anhui, China

³ University of Science and Technology of China, Hefei 230026, Anhui, China

* Correspondence: Christa.Fittschen@univ-lille.fr

Abstract: The absolute absorption cross section of the ethyl peroxy radical, C₂H₅O₂, in the $\tilde{A} \leftarrow \tilde{X}$ electronic transition with the peak wavelength at 7596 cm⁻¹, has been determined by the method of dual wavelengths time resolved continuous wave cavity ring down spectroscopy. C₂H₅O₂ radicals were generated from pulsed 351 nm photolysis of C₂H₆/Cl₂ mixture in presence of O₂ and detected on one of the CRDS paths. Two methods have been applied for the determination of the C₂H₅O₂ absorption cross section: (i) based on Cl-atoms being converted alternatively to either C₂H₅O₂ by adding C₂H₆ or to hydro peroxy radicals, HO₂, by adding CH₃OH to the mixture, whereby HO₂ was reliably quantified on the second CRDS path in the 2v₁ vibrational overtone at 6638.2 cm⁻¹ (ii) based on the reaction of C₂H₅O₂ with HO₂, measured under either excess HO₂ or under excess C₂H₅O₂ concentration. Both methods lead to the same peak absorption cross section of $\sigma_{\text{C}_2\text{H}_5\text{O}_2, 7596 \text{ cm}^{-1}} = (1.0 \pm 0.2) \times 10^{-20} \text{ cm}^2$. The rate constant for the cross reaction between of C₂H₅O₂ and HO₂ has been measured to be $(6.5 \pm 1.6) \times 10^{-12} \text{ cm}^3 \text{ molecule}^{-1} \text{ s}^{-1}$.

Keywords: Peroxy radicals, near-infrared spectroscopy, $\tilde{A} \leftarrow \tilde{X}$ electronic transition, cavity ring down spectroscopy

1. Introduction

The oxidation of volatile organic compounds (VOCs) in the troposphere is mainly driven by hydroxyl radicals (OH) and leads, after addition of O₂, to the formation of organic peroxy radicals (RO₂). The fate of these RO₂ radicals depends on the chemical composition of the environment. In a polluted atmosphere they react mainly with nitric oxide (NO) to form alkoxy radicals or react with nitrogen dioxide (NO₂) to form peroxy nitrates (RO₂NO₂). Subsequent to the reaction with NO, alkoxy radicals react with O₂ to form hydro peroxy radicals (HO₂). HO₂ further oxidises NO into NO₂ and thus regenerates OH, closing the quasi-catalytic cycle. The photolysis of produced NO₂ is the only relevant chemical source of tropospheric ozone. In clean environments with low NO_x (NO_x = NO + NO₂) concentrations, the dominant loss of RO₂ is due to its reaction with HO₂ forming hydroperoxides ROOH and terminating the radical reaction chain. In addition, RO₂ radicals can react either with themselves as self-reaction (RO₂ + RO₂) or with other R'O₂ as cross-reaction (RO₂ + R'O₂) or with OH radicals (RO₂ + OH) [1-5].

Ethane is one of the most abundant non-methane hydrocarbons in the atmosphere, and its atmospheric oxidation leads to the formation of the ethyl peroxy radical, C₂H₅O₂. A reliable detection of this radical is therefore highly desirable for studying its reactivity

and thus understanding its embedded chemistry. Previous studies of peroxy chemistry have mostly been carried out by UV absorption spectroscopy in the $\tilde{B} \leftarrow \tilde{X}$ electronic transition: this method gives a good sensitivity for peroxy radicals due to large absorption cross sections, but the selectivity is poor because the absorption spectra are unstructured and the spectra of many different species are overlapping.

The $\tilde{A} \leftarrow \tilde{X}$ electronic transition of peroxy radicals is located in the near IR region and allows a more selective detection of peroxy radicals, compared to UV absorption. However, due to small absorption cross sections ($\sim 10^{-20}$ – 10^{-21} cm²), these transitions have not attracted much attention after they had been located for the first time by Hunziker and Wendt in 1976 [6,7]. Interest has been revived many years later when the highly sensitive absorption technique of cavity ring down spectroscopy (CRDS) has been developed [8,9], which can make up for the small absorption cross sections. The first report on using this technique for the detection of peroxy radicals was in 2000 [10]: T. Miller and coworkers obtained pulsed near IR radiation by stimulated Raman shifting of the output of a pulsed dye laser in molecular hydrogen. They measured the absorption spectra of the methyl and ethyl peroxy radicals, but determined only the absorption cross section for the methyl peroxy radical. The peak of the $\tilde{A} \leftarrow \tilde{X}$ transition for C₂H₅O₂ was found around 7596 cm⁻¹.

A few years later, Atkinson and Spillman [11] measured again the spectra of both radicals, now using a continuous external cavity diode laser to perform cw-CRDS. They confirmed the overall shape of the absorption spectrum, and measured for the first time the absorption cross section for C₂H₅O₂ using the kinetic method [12-15]. This method can be applied, if the rate constant of a radical-radical reaction is known, because the initial concentration and thus the absorption cross section can in principle be determined from the shape of the kinetic decay. The self-reaction can be described as follows



$$\frac{d[A]}{dt} = -2k[A]^2 \quad [\text{Eq. 1}]$$

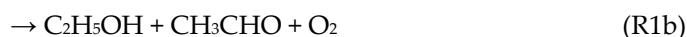
Integration of [Eq. 1] leads to

$$\frac{1}{[A]} = \frac{1}{[A]_0} + 2kt \quad [\text{Eq. 2}]$$

Hence, plotting $1/[A]$ as a function of time leads to a straight line with the slope being $2k$. In the case where the rate constant is known, but not the absolute concentration of A, the absorption coefficient $\alpha = \sigma \times [A]$ can be used in [Eq. 2] instead of $[A]$, leading to

$$\frac{1}{\sigma \times [A]} = \frac{1}{\sigma \times [A]_0} + \frac{2k}{\sigma} t \quad [\text{Eq. 3}]$$

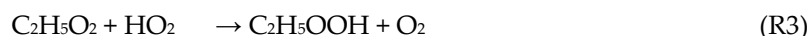
Plotting $1/\sigma \times [A]$ leads to a straight line with the slope being $m = 2k / \sigma$ while the intercept $I = 1/\sigma \times [A]_0$. However, different complications can arise from this method: radicals can be lost through other processes too, for example through diffusion out of the photolysed volume or through unidentified secondary reactions in which case the decays are faster than expected from pure self-reaction only, and the retrieved absorption cross section would be too small. In the case of peroxy radicals, this method has another complication: the self-reaction of peroxy radicals has several product pathways, and one of them leads to the formation of HO₂ radicals:



and, in presence of O₂:



The HO₂ radicals react with C₂H₅O₂



with (R3) having a rate constant faster than (R1). As a result, the $\text{C}_2\text{H}_5\text{O}_2$ decays are accelerated by the formation of HO_2 , and therefore when using [Eq. 3] for (R1), the obtained rate constant k_1 is called $k_{1,obs}$ and the acceleration has to be taken into account to retrieve the “real” rate constant k_1 from $\text{C}_2\text{H}_5\text{O}_2$ decays. Using the recommended value of $k_{1,obs}$ in the kinetic method, Atkinson and Spillman [11] obtained an absorption cross section of $\sigma_{\text{C}_2\text{H}_5\text{O}_2, 7596 \text{ cm}^{-1}} = (3.0 \pm 1.5) \times 10^{-21} \text{ cm}^2$.

Another work on the ethyl peroxy spectrum from the Miller group [16] used a different method to estimate the absorption cross section: peroxy radicals were generated by the reaction of Cl-atoms with C_2H_6 , with the Cl-atoms being generated by 193 nm photolysis of oxalylchloride, $(\text{COCl})_2$. To obtain the concentration of $\text{C}_2\text{H}_5\text{O}_2$, they measured the photolysis laser energy with and without precursor, and calculated the Cl-atom concentration from the difference. Supposing that each Cl-atom generated one $\text{C}_2\text{H}_5\text{O}_2$ radical, they obtained $\sigma_{\text{C}_2\text{H}_5\text{O}_2, 7596 \text{ cm}^{-1}} = 4.4 \times 10^{-21} \text{ cm}^2$.

The next work on the ethyl peroxy spectrum from the Miller group [17] used a different method to obtain the absorption cross section: in a dual-path CRDS set-up, the concentration of HCl (generated from the reaction of Cl-atoms with C_2H_6) was measured on one path while the absorption of $\text{C}_2\text{H}_5\text{O}_2$ was measured simultaneously on the other path. Again supposing that each HCl-molecule had generated one $\text{C}_2\text{H}_5\text{O}_2$ radical, they obtained $\sigma_{\text{C}_2\text{H}_5\text{O}_2, 7596 \text{ cm}^{-1}} = (5.29 \pm 0.20) \times 10^{-21} \text{ cm}^2$.

In the most recent work from the Miller group [18], the above absorption cross section was validated indirectly through the kinetic method: the $\text{C}_2\text{H}_5\text{O}_2$ absorption profiles were converted to $\text{C}_2\text{H}_5\text{O}_2$ concentration-time profiles using the above absorption cross section, and the rate constant $k_{1,obs}$ for the self-reaction was extracted. Good agreement with other literature data was found, which was taken as an indication that the absorption cross section is valid. A summary of previous results as well as the results obtained in this work is presented in **Table 1**.

Table 1: Summary of the $\text{C}_2\text{H}_5\text{O}_2$ absorption cross section at 7596 cm^{-1}

$\sigma / 10^{-21} \text{ cm}^2$	Method	Reference
3.0 ± 1.5	Kinetic method, no other radical losses considered	Atkinson and Spillman [11]
4.4	Depletion of photolysis energy through precursor with $[\text{Cl}] = [\text{C}_2\text{H}_5\text{O}_2]$, i.e. no secondary reactions considered	Rupper et al. [16]
5.29 ± 0.20	Measurement of HCl in dual path CRDS with $[\text{Cl}] = [\text{C}_2\text{H}_5\text{O}_2]$, i.e. no secondary reactions considered	Melnik et al. [17]
5.29	Kinetic method used for validation of Ref [17]	Melnik et al. [18]
10 ± 2	Measurement of HO_2 / $\text{C}_2\text{H}_5\text{O}_2$ in dual path CRDS with $[\text{Cl}] = [\text{HO}_2] = [\text{C}_2\text{H}_5\text{O}_2]$	This work
10 ± 2	Kinetic method from $\text{C}_2\text{H}_5\text{O}_2 + \text{HO}_2$	This work

In this work we present a new determination of the absorption cross section, based on two different approaches. The first one is comparable to one of the Miller methods [17] and will be called back-to-back method: in our dual-path CRDS set-up we generate Cl-atoms and transform them to HO_2 through reaction with CH_3OH , with HO_2 being quantified on one path at 6638.2 cm^{-1} . Shortly after, the Cl-atoms were transformed to $\text{C}_2\text{H}_5\text{O}_2$ by adding C_2H_6 instead of CH_3OH to the reaction mixture and the $\text{C}_2\text{H}_5\text{O}_2$ absorption was

measured on the second path. Supposing that the Cl concentration stays the same between both experiments and that in both cases all Cl-atoms are converted to either HO₂ (which can be quantified reliably) or to C₂H₅O₂, the absorption cross section of C₂H₅O₂ is determined relative to the one of HO₂. The second approach is a variation of the kinetic method such as used by Atkinson and Spillman [11] and Melnik *et al.* [18], but not based on the self-reaction of C₂H₅O₂, but on the cross reaction between HO₂ and C₂H₅O₂. This reaction has been measured in a wide range of concentrations under either excess of HO₂ or excess of C₂H₅O₂. In the first case, the rate constant is retrieved by adjusting the C₂H₅O₂ decays with the absolute concentration of HO₂ being fixed, while in the second case the rate constant is fixed to the value determined just before, and now the best fit of the HO₂ decay is achieved by adjusting the absolute concentration of C₂H₅O₂, i.e. the absorption cross section.

2. Materials and Methods

The setup has been described in detail before [19–22] and is only briefly discussed here (Figure 1).

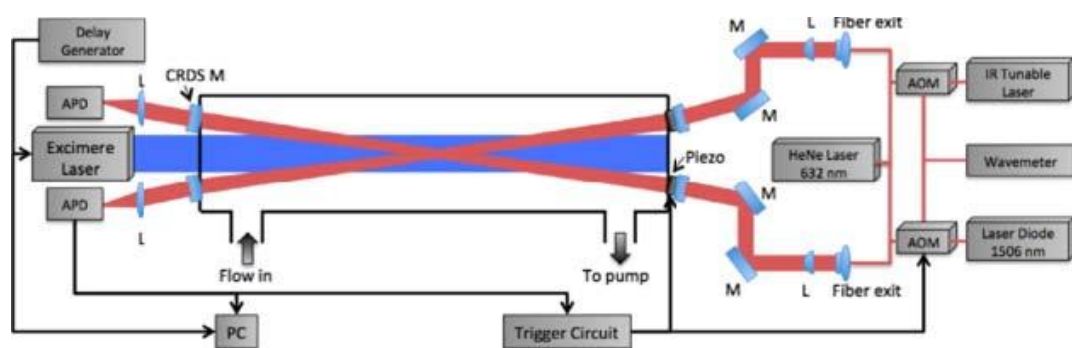


Figure 1. Schematic view of the used experimental setup: AOM, Acousto-Optic Modulator; APD, Avalanche Photo Diode; M, Mirror; L, Lens. Both cw-CRDS systems are equipped with identical trigger circuits and data acquisition systems.

The setup consisted of a 0.79 m long flow reactor made of stainless steel. The photolysis laser (Lambda Physik LPX 202i, XeF at 351 nm) width is delimited to 2 cm and passes through the reactor longitudinally. The flow reactor contains two identical continuous wave cavity ring-down spectroscopy (cw-CRDS) absorption paths, which were installed in a small angle with respect to the photolysis path. An overlap of the absorption path with the photolysis beam of 0.288 m is achieved. Both beam paths were tested for a uniform overlap with the photolysis beam before experiments were done. For this purpose, both cw-CRDS instruments were operated to simultaneously measure HO₂ concentrations. Deviations between HO₂ concentrations were less than 5 % demonstrating that the photolysis laser was very well aligned, *i.e.* both light paths probed a very similar photolysed volume in the reactor. A small helium purge flow prevented the mirrors from being contaminated. Two different DFB lasers are used for the detection of the two species and each one is coupled into one of the cavities by systems of lenses and mirrors. Each probe beam passed an acousto-optic modulator (AOM, AAoptoelectronic) to rapidly turn off the 1st order beam once a user-set threshold for light intensity in the cavity was reached, in order to measure the ring-down event. A home-made tracking system is used to increase the number of ring-down events [23]. Then, the decay of light intensity is recorded and an exponential fit is applied to retrieve the ring-down time. The absorption coefficient α is derived from [Eq. 4].

$$\alpha = [A] \times \sigma_A = \frac{R_L}{c} \left(\frac{1}{\tau} - \frac{1}{\tau_0} \right) \quad [\text{Eq. 4}]$$

where τ is the ring-down time with an absorber present; τ_0 is the ring-down time with no absorber present; σ_A is the absorption cross section of the absorbing species A; R_L is the

ratio between cavity length (79 cm) and effective absorption path (28.8 cm); c is the speed of light.

Ethyl peroxy radicals were generated by pulsed 351 nm photolysis of C_2H_6 / Cl_2 / O_2 mixtures:



For studying the cross reaction with HO_2 , methanol, CH_3OH , has been added in varying concentrations to the mixture.



In order to rapidly convert $\text{C}_2\text{H}_5\text{O}$ into HO_2 through (R2), all experiments have been carried out in 100 Torr O_2 (Air Liquide, Alphagaz 2)

A small flow of pure ethane was added directly from the cylinder (Mitry-Mory, N35) to the mixture through a calibrated flow meter (Bronkhorst, Tylan). Methanol (Sigma-Aldrich) was added to the mixture by flowing a small fraction of the main flow through a bubbler containing liquid methanol, kept in ice or in a thermostated water bath. All experiments were carried out at 298 K.

3. Results

In the following, the two different methods applied in this work for the determination of the absorption cross section of $\text{C}_2\text{H}_5\text{O}_2$ at its peak wavelength 7596 cm^{-1} are described.

3.1. Quantification of $\text{C}_2\text{H}_5\text{O}_2$ in back-to-back experiments

In the first method, the absorption cross section of $\text{C}_2\text{H}_5\text{O}_2$ is measured in a rather direct way in back-to-back experiments relative to the absorption cross section of HO_2 . Therefore, the reliability of the measurement depends on the reliability of the absorption cross section of HO_2 . The absorption spectrum and cross sections of HO_2 in the near IR have been measured several times [22,24-26] and pressure broadening of selected lines has also been carried out [27-29]. In this work, HO_2 was quantified on two different absorption lines with the cross section varying about a factor of 9 between both lines: for most experiments, HO_2 has been detected on the strongest line of the $2\nu_1$ band at 6638.2 cm^{-1} , but for experiments with high initial radical concentrations a small line at 6638.58 cm^{-1} has been used to avoid saturation. The absorption cross section of the strongest line in helium ($\sigma_{50\text{ Torr He}} = 2.72 \times 10^{-19}\text{ cm}^2$) [24,25] and in synthetic air [$\sigma_{100\text{ Torr air}} = 1.44 \times 10^{-19}\text{ cm}^2$] has been measured several times, the cross section of the small line has only been measured once in 50 and 100 Torr helium (2.8 and $2.1 \times 10^{-20}\text{ cm}^2$, respectively) [31], but no measurements in pure O_2 have been carried out. Therefore, we have determined both cross sections in 100 Torr O_2 in the frame of this work, using the kinetic method.

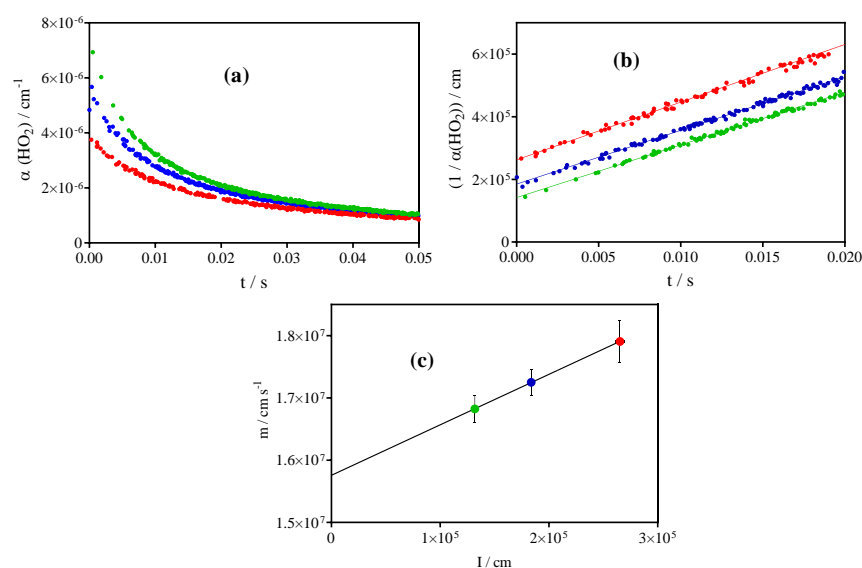


Figure 2. Example of measurement of HO₂ absorption cross section using the kinetic method: graph (a) shows kinetic decays for 3 different Cl-atom concentrations, graph (b) shows the same signals plotted following [Eq. 3] with the linear regression over the first 20 ms, graph (c) shows the plot of slope m as a function of I , obtained in graph (b) for the 3 experiments.

Figure 2 shows a typical example: HO₂ decays have been measured for 3 different initial Cl-atom concentrations and the raw signals are presented in graph (a). The decays have then been plotted following [Eq. 3] and the result is shown in graph (b). The slope of a linear regression of this plot can in principle be converted to the absorption cross section using the known rate constant of the HO₂ self-reaction. However, as has been mentioned above, radicals can be lost also through other processes, and in the case of laser photolysis experiments one possible loss is diffusion out of the photolysis volume. The relative impact of this loss process decreases with increasing initial HO₂ concentration and in order to correct this influence, an extrapolation to infinite [HO₂]₀ is used, shown in graph (c): the slope m from graph (b) is plotted as a function of the intercept I ($=1/\alpha_0$). Extrapolating the m -values to $I = 0$ therefore removes the influence of the diffusion on the slope m . In the example of **Figure 2**, using the slope m obtained from extrapolation instead of using the directly determined slope m leads to an increase in the absorption cross section of 6% for the highest concentration and 13% for the lowest concentration. Error bars in graph (c) correspond to 95% confidence interval of the linear regression from the graph (b): the error bars on the x-values are too small to be seen within the symbols. Several such series have been measured for both absorption lines, and the following absorption cross sections in 100 Torr O₂ have been deduced for the two lines:

$$\sigma_{\text{HO}_2, 6638.2 \text{ cm}^{-1}} = (2.0 \pm 0.3) \times 10^{-19} \text{ cm}^2$$

$$\sigma_{\text{HO}_2, 6638.58 \text{ cm}^{-1}} = (2.1 \pm 0.3) \times 10^{-20} \text{ cm}^2.$$

The uncertainty on σ reflect the uncertainty of $\pm 15\%$ on the rate constant of the HO₂ self-reaction, such as estimated by the IUPAC committee [32].

These absorption cross sections are now used to obtain the absorption cross section of C₂H₅O₂ in back-to-back experiments. **Figure 3** shows the principle of these measurements: Cl₂ is first photolysed in the presence of excess CH₃OH, leading to quantitative formation of HO₂ radicals: typical absorption-time profiles for 4 different Cl₂ concentrations are shown in the upper right graph (b) of **Figure 3**. In the next step, CH₃OH is removed from the gas flow, and excess C₂H₆ is added instead, all other conditions are kept constant. The corresponding C₂H₅O₂ absorption time profiles are shown in the upper left graph (a). It can be seen that the HO₂ profiles decay much faster than the corresponding

$C_2H_5O_2$ profiles: this is in line with the rate constant of the HO_2 self-reaction being around 10 times faster than the rate constant of the $C_2H_5O_2$ self-reaction. In order to get a reliable extrapolation of $\alpha_{t=0ms}$, a plot of $1/\alpha = f(t)$ is generated for both species (graph (c) and (d) for $C_2H_5O_2$ and HO_2 , respectively) and a linear regression allows retrieving $\alpha_{t=0ms}$ from the intercept, as shown in [Eq. 3]. $\alpha_{HO_2, t=0ms}$ values can now be converted to absolute concentrations ($[HO_2]_{t=0ms}$) using the above determined absorption cross section. Supposing that each Cl-atom is converted into either one HO_2 radical or into one $C_2H_5O_2$ radical, *i.e.* $[HO_2]_{t=0ms} = [C_2HO_5]_{t=0ms}$, a plot of $\alpha_{C_2H_5O_2, t=0ms} = f([HO_2]_{t=0ms})$ leads to a linear relationship with the slope equal to the absolute absorption cross section of $C_2H_5O_2$. The lower graph (e) in **Figure 3** summarizes the results, obtained on four different days using either the big HO_2 line at 6638.2 cm^{-1} (open circles and open diamonds) or the small line at 6635.58 cm^{-1} (all other symbols, with the coloured symbols representing the results from the experiment in **Figure 3**).

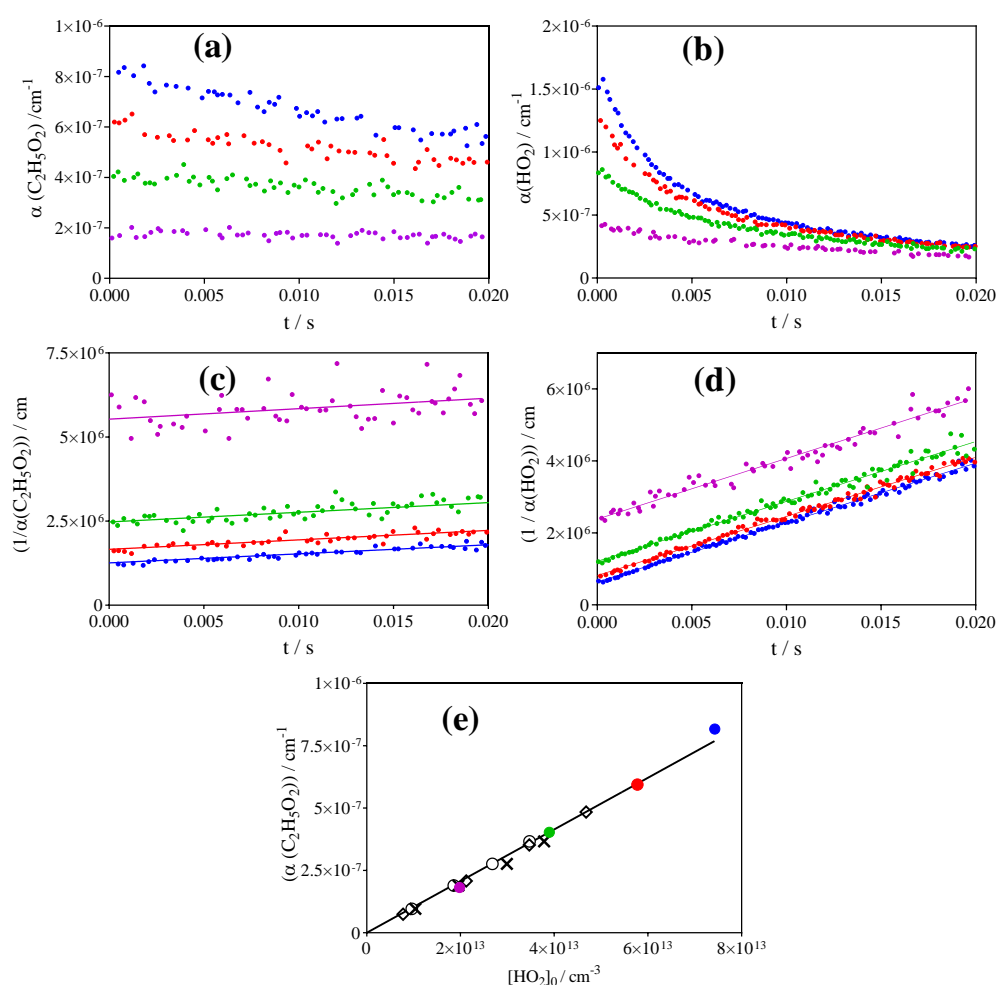


Figure 3. Example of measurement of the $C_2H_5O_2$ absorption cross section relative to the HO_2 absorption cross section. Upper graphs: $C_2H_5O_2$ (a) and HO_2 (b) absorption time profiles. Graphs (c) and (d): same profiles, converted to $1/\alpha$ (see [Eq. 3]) and linear regression over the first 20 ms following the photolysis pulse. Lower graph (e) shows plot of $\alpha_{(C_2H_5O_2)t=0ms} = f([HO_2]_{t=0ms})$: open circles and open diamonds are obtained using HO_2 measurements at 6638.2 cm^{-1} , coloured points (from above graphs), crosses are obtained using HO_2 measurements at 6635.58 cm^{-1} . $[O_2] = 2.8 \times 10^{18}\text{ cm}^{-3}$, $[C_2H_6] = 3.7 \times 10^{16}\text{ cm}^{-3}$ for all experiments.

From these experiments, we obtain an absorption cross section for $C_2H_5O_2$ of $\sigma_{C_2H_5O_2, 7596\text{ cm}^{-1}} = (1.0 \pm 0.2) \times 10^{-20}\text{ cm}^2$. The error bar is mostly due to the uncertainty in the rate

constant of the HO₂ self-reaction, to which the absorption cross section of C₂H₅O₂ is directly linked.

In imitation of the kinetic method such as used by Melnik *et al.*[18], the above experiments can also be used to validate the absorption cross section obtained using the back-to-back method by determining $k_{3,obs}$ and comparing it with data from the literature. Indeed, the C₂H₅O₂ data from **Figure 3(c)** can be treated with the same method as shown for the HO₂ data in **Figure 2**, and the obtained intercept is then equal to $2 \times k_{obs} / \sigma$. **Figure 4** shows this type of plot for the data from **Figure 3(c)**.

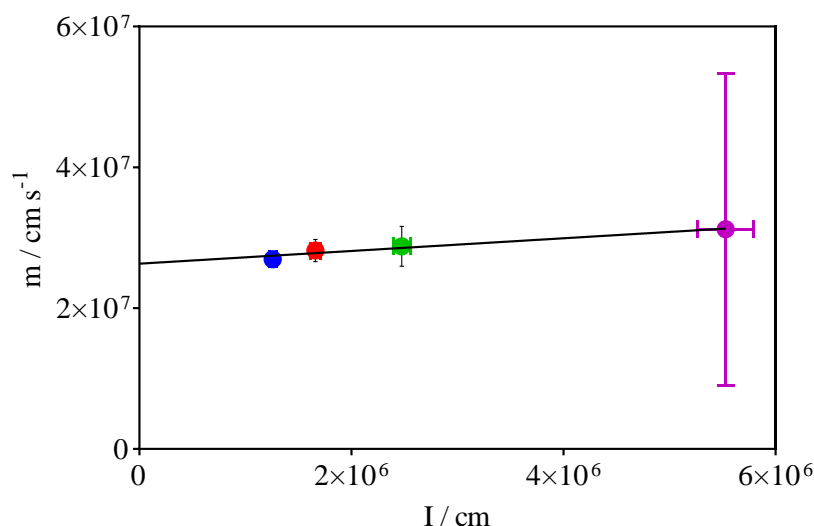


Figure 4. Plot of slope m as a function of I from the linear regressions obtained in **Figure 3 (c)**.

Now, using the above retrieved absorption cross section of $\sigma_{\text{C}_2\text{H}_5\text{O}_2, 7596 \text{ cm}^{-1}} = (1.0 \pm 0.2) \times 10^{-20} \text{ cm}^2$, we can obtain from the intercept of the linear regression in **Figure 4** a value for $k_{1,obs} = (1.3 \pm 0.3) \times 10^{-13} \text{ cm}^3 \text{ molecule}^{-1} \text{ s}^{-1}$, in good agreement with the currently recommended literature value ($1.24 \times 10^{-13} \text{ cm}^3 \text{ molecule}^{-1} \text{ s}^{-1}$) [33].

3.2. Quantification of C₂H₅O₂ by measuring the rate constant of C₂H₅O₂ + HO₂

Another way to determine the absorption cross-section of C₂H₅O₂ has been applied by determining the rate constant of the cross reaction between C₂H₅O₂ and HO₂. Indeed, the rate constant can be determined under different conditions: using an excess of HO₂ over C₂H₅O₂ leads to C₂H₅O₂ decays that are sensitive to the absolute concentration of HO₂, while in the reverse case the HO₂ decay will be sensitive to the absolute C₂H₅O₂ concentration, and thus to its absorption cross section. Therefore, measuring simultaneously the decays of both species over a large range of concentration ratio allows determining the rate constant (from excess HO₂ experiments) and the absorption cross section of C₂H₅O₂ (from excess C₂H₅O₂ experiments). **Figure 5** presents results from such an experiment with an initial Cl-atom concentration of $1.2 \times 10^{14} \text{ cm}^{-3}$ for all experiments, obtained in initial experiments from measuring pure HO₂ decays (no C₂H₆ added). [C₂H₆] has been varied between $1.9 - 7.5 \times 10^{14} \text{ cm}^{-3}$ and [CH₃OH] has been varied between $2.4 - 5.3 \times 10^{15} \text{ cm}^{-3}$. Using these conditions, the ratio of [HO₂] / [C₂H₅O₂] has been varied between 0.2 (pink circles) and 3 (black circles).

Both species show different behaviour: C₂H₅O₂ always decreases rapidly over the first few ms, given by the loss through (R3). Then the decays slow down at longer reaction times, when HO₂ concentration gets low, because the self-reaction becomes the major loss reaction, and this reaction is slow for C₂H₅O₂ radicals. This behaviour is especially visible when C₂H₅O₂ is the excess species (pink circles: [C₂H₅O₂] $\approx 4 \times$ [HO₂]). HO₂ on the other hand approaches low concentrations at longer reaction times under all conditions, even when it is the excess species (black circles: [HO₂] $\approx 3 \times$ [C₂H₅O₂]): its self-reaction is much

faster than the self-reaction of $\text{C}_2\text{H}_5\text{O}_2$ and is a major loss process under all conditions and all reaction times. The profiles have simultaneously been fitted to a simple mechanism, given in **Table 2**.

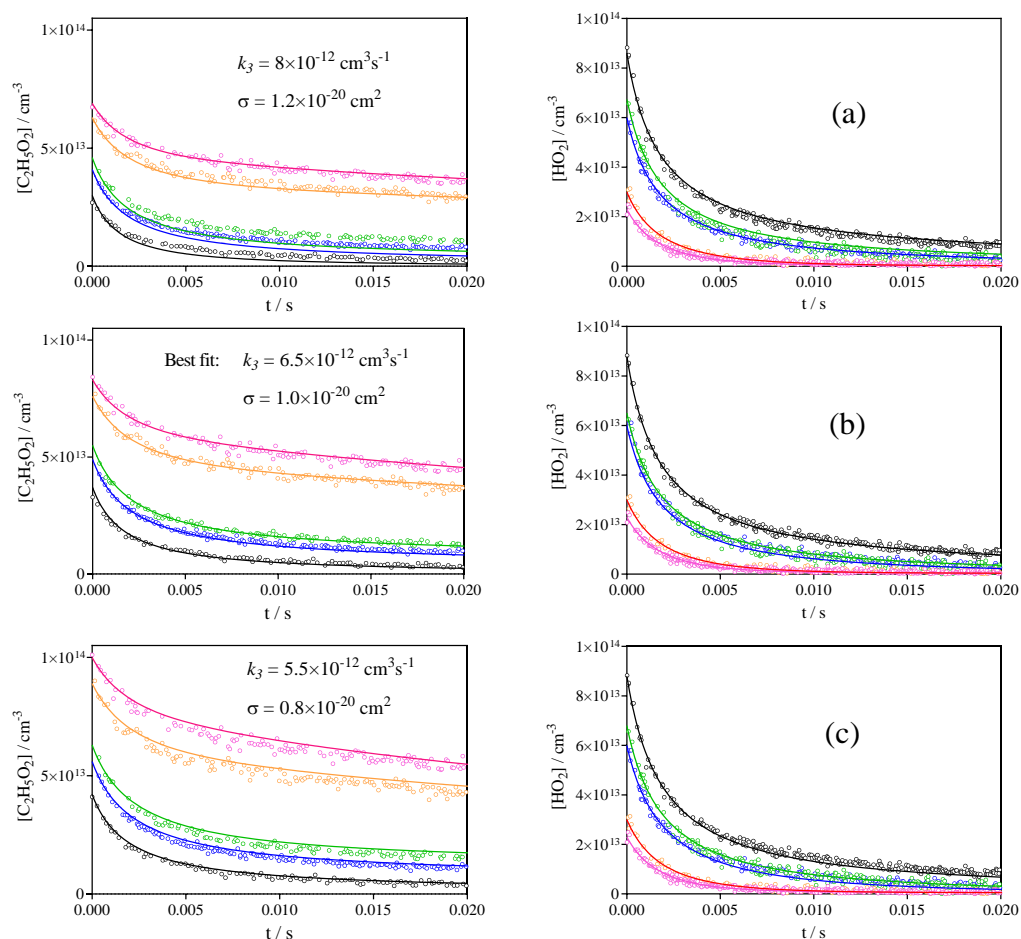


Figure 5. $\text{C}_2\text{H}_5\text{O}_2$ (left graphs) and HO_2 (right graphs) concentration time profiles for a total radical concentration of $1.2 \times 10^{14} \text{ cm}^{-3}$. Centre graphs (b): best fit with $k_3 = 6.5 \times 10^{-12} \text{ cm}^3 \text{ molecule}^{-1} \text{ s}^{-1}$, and $\sigma_{\text{C}_2\text{H}_5\text{O}_2, 7596 \text{ cm}^{-1}} = 1.0 \times 10^{-20} \text{ cm}^2$, upper graphs (a): model with upper limit of k_3 and σ , lower graphs (c): model with lower limit of k_3 and σ

For the centre graphs (b) in **Figure 5**, the above determined absorption cross section ($\sigma_{\text{C}_2\text{H}_5\text{O}_2, 7596 \text{ cm}^{-1}} = 1.0 \times 10^{-20} \text{ cm}^2$) has been used to convert the $\text{C}_2\text{H}_5\text{O}_2$ absorption coefficients into absolute concentrations. The profiles for both species could be well reproduced over the entire concentration range using a rate constant of $k_3 = 6.5 \times 10^{-12} \text{ cm}^3 \text{ molecule}^{-1} \text{ s}^{-1}$. In a next step, different rate constants for the cross reaction have been tested: indeed, despite several measurements of this rate constant over the last decades [34–40], there is no good agreement for this rate constant. An excellent summary on previous measurements of this rate constant can be found in Noell *et al.* [34] and will not be repeated here. The two recent determinations from Noell *et al.* [34] and Boyd *et al.* [35] are considered by the IUPAC committee as being carried out by the most reliable methods, however they vary by about a factor of 1.5 ($8.14 \times 10^{-12} \text{ cm}^3 \text{ molecule}^{-1} \text{ s}^{-1}$ for Boyd *et al.* [35] from UV absorption and $5.57 \times 10^{-12} \text{ cm}^3 \text{ molecule}^{-1} \text{ s}^{-1}$ for Noell *et al.* [34] from UV / near IR absorption). We have tested these two limits by trying to adjust both profiles over the entire concentration range: indeed, the profile obtained by the model using an increased rate constant can be compensated for in a certain limit through decreased concentration (*i.e.* increased absorption cross section) of the excess species and vice versa. In the upper graphs (a), the upper limit has been tested by setting $k_3 = 8 \times 10^{-12} \text{ cm}^3 \text{ molecule}^{-1} \text{ s}^{-1}$. Now, the absorption cross section

needs to be increased by around 20% ($\sigma_{\text{C}_2\text{H}_5\text{O}_2, 7596 \text{ cm}^{-1}} = 1.2 \times 10^{-20} \text{ cm}^2$) to obtain lower $\text{C}_2\text{H}_5\text{O}_2$ concentrations in order to slow down the HO_2 decays. However, after a few ms both profiles are not well reproduced anymore: HO_2 concentrations are slightly too high, while the $\text{C}_2\text{H}_5\text{O}_2$ concentrations are clearly too low for all concentration ratios: this is due to the fact, that with the larger absorption cross section the initial dip in the $\text{C}_2\text{H}_5\text{O}_2$ concentration is smaller than the initial HO_2 concentration. In the lower graphs (c), the rate constant k_3 has been set to the lower limit such as obtained by Noell *et al.* [34] ($5.5 \times 10^{-12} \text{ cm}^3 \text{ molecule}^{-1} \text{ s}^{-1}$). Now, HO_2 decays are now much too slow compared to the model in the upper graphs, and therefore the initial $\text{C}_2\text{H}_5\text{O}_2$ concentration needs to be increased by about 20% (corresponding to a decreased absorption cross section: $\sigma_{\text{C}_2\text{H}_5\text{O}_2, 7596 \text{ cm}^{-1}} = 0.8 \times 10^{-20} \text{ cm}^2$). Using these parameters, acceptable HO_2 decays can be obtained (even though slightly too low at longer reaction times), however the $\text{C}_2\text{H}_5\text{O}_2$ profiles cannot be reproduced anymore: the fast decay over the first few ms does not go deep enough, the model predicts too high $\text{C}_2\text{H}_5\text{O}_2$ concentrations at longer time scales for all concentration ratios. This is due to the fact, that the absolute dip of $\text{C}_2\text{H}_5\text{O}_2$ is higher than the initial HO_2 concentration

Table 2: Reaction mechanism used to fit all experiments in this work

	Reaction	$k / \text{cm}^3 \text{ molecule}^{-1} \text{ s}^{-1}$	Reference
1a	$2 \text{ C}_2\text{H}_5\text{O}_2 \rightarrow 2 \text{ C}_2\text{H}_5\text{O} + \text{O}_2$	2.6×10^{-14}	Ref [34]
1b	$2 \text{ C}_2\text{H}_5\text{O}_2 \rightarrow \text{C}_2\text{H}_5\text{OH} + \text{CH}_3\text{CHO} + \text{O}_2$	6.7×10^{-14}	Ref [34]
2	$\text{C}_2\text{H}_5\text{O} + \text{O}_2 \rightarrow \text{CH}_3\text{CHO} + \text{HO}_2$	8×10^{-15}	Ref[41]
3	$\text{C}_2\text{H}_5\text{O}_2 + \text{HO}_2 \rightarrow \text{C}_2\text{H}_5\text{OOH} + \text{O}_2$	6.5×10^{-12}	This work
5	$\text{Cl} + \text{C}_2\text{H}_6 \rightarrow \text{C}_2\text{H}_5 + \text{HCl}$	5.9×10^{-11}	Ref[33]
6a	$\text{C}_2\text{H}_5 + \text{O}_2 + \text{M} \rightarrow \text{C}_2\text{H}_5\text{O}_2 + \text{M}$	4.8×10^{-12}	Ref[42]
6b	$\text{C}_2\text{H}_5 + \text{O}_2 \rightarrow \text{C}_2\text{H}_4 + \text{HO}_2$	$3\text{--}4 \times 10^{-14}$	This work
7	$\text{Cl} + \text{CH}_3\text{OH} \rightarrow \text{CH}_2\text{OH} + \text{HCl}$	5.5×10^{-11}	Ref[33]
8	$\text{CH}_2\text{OH} + \text{O}_2 \rightarrow \text{CH}_2\text{O} + \text{HO}_2$	9.6×10^{-12}	Ref[33]
9	$2 \text{ HO}_2 \rightarrow \text{H}_2\text{O}_2 + \text{O}_2$	1.7×10^{-12}	Ref [32]
10	$\text{C}_2\text{H}_5\text{O}_2 \rightarrow \text{diffusion}$	2 s^{-1}	This work
11	$\text{HO}_2 \rightarrow \text{diffusion}$	3 s^{-1}	This work

The absorption cross section for $\text{C}_2\text{H}_5\text{O}_2$ obtained in these experiments is in good agreement with the one obtained in back-to-back experiments, described above. However, it should of course be noted, that in the end both methods rely on the absorption cross section of HO_2 and therefore both approaches cannot be considered as independent methods. The change in the absorption cross section of HO_2 varies through pressure broadening (which is taken into account), but it might also vary during the experiment through small and unnoted shifts in the wavelength of the DFB laser emission (the linewidth of the HO_2 absorption lines are on the order of 0.02 cm^{-1} FWHM at 50 Torr he). However, in our experiments the absorption cross section of HO_2 is under most conditions constantly being “measured”: a major HO_2 loss in most experiments is the self-reaction, and thus the HO_2 decays are sensitive to the absolute HO_2 concentration, *i.e.* to the absorption cross section that has been used to convert the absorption time profiles to concentration time profiles. Therefore, it can be said that both methods have determined the $\text{C}_2\text{H}_5\text{O}_2$ absorption cross section relative to the rate constant of the HO_2 self-reaction. The IUPAC committee [32] estimates the uncertainty of this rate constant to $\pm 15\%$, which we use as a basis

to estimate the uncertainty of our rate constant, with an additional 10% for uncertainties in the fitting of the rate constant: $k_3 = (6.5 \pm 1.6) \times 10^{-12} \text{ cm}^3 \text{ molecule}^{-1} \text{ s}^{-1}$.

3.3 Measuring the relative absorption spectrum

In order to obtain the shape of the $\text{C}_2\text{H}_5\text{O}_2$ absorption spectrum, kinetic decays have been measured under identical conditions at 15 different wavelengths in the range accessible with our DFB laser ($7596 - 7630 \text{ cm}^{-1}$). The relative absorption coefficients are put on an absolute scale by comparison with the absorption cross section at 7596.47 cm^{-1} . **Table 3** summarizes the obtained results, and **Figure 6** compares the present data with two literature results. The upper graph shows that our spectrum (green symbols and green axis apply) agrees well with the results of Melnik *et al.*[17] if our data are shifted by 4 cm^{-1} . Possibly, there is a mistake in the Melnik figure (T. Miller, private communication), because the peak absorption is given in the text at 7496 cm^{-1} , just as in our case, however in the figure the peak is located at 7600 cm^{-1} , indicated by a blue vertical line. In the lower graph, our data (again in green) are overlaid to the spectrum of Atkinson and Spillman [11]. A good agreement of the shape in both comparisons can be obtained, when our data are squeezed, *i.e.* when we suppose a shift in the baseline of both literature spectra. Melnik *et al.* observed such baseline shift (dashed line in their figure) and attributed it to a broadband absorber, generated simultaneously during the photolysis. No explanation for a possible baseline shift in the work of Atkinson and Spillman can be given.

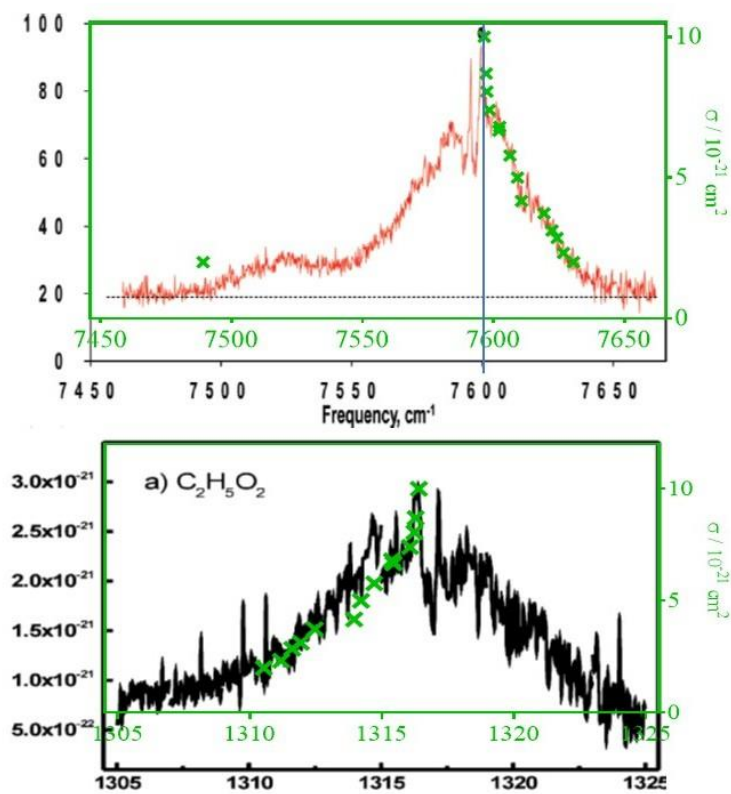


Figure 6. $\text{C}_2\text{H}_5\text{O}_2$ absorption coefficients at different wavelengths obtained in this work (green crosses and green axis), overlaid onto the spectrum obtained by Melnik *et al.* [17] (upper graph, Reprinted with permission from [17], Copyright 2010 American Chemical Society) and Atkinson and Spillman [11] (lower graph, Reprinted with permission from [11], Copyright 2002 American Chemical Society). In the upper graph the data have been shifted by 4 cm^{-1} , and in both graphs our data have to be squeezed together, *i.e.* apparently there is a baseline shift in both comparisons.

Table 3: $\text{C}_2\text{H}_5\text{O}_2$ Absorption cross sections at different wavelengths

Wavenumber / cm^{-1}	$\sigma / 10^{-20} \text{ cm}^2$
-------------------------------	----------------------------------

7596.47	10.0
7597.20	8.7
7597.44	8.1
7598.40	7.4
7602.02	6.7
7602.38	6.8
7606.25	5.8
7609.16	5.0
7610.66	4.2
7619.28	3.7
7622.36	3.1
7624.28	2.9
7626.72	2.3
7630.50	2.0
7489.16	2.0

4. Discussion

4.1. Comparison of the absorption cross section with literature data

The absorption cross section was first determined by Atkinson and Spillman [11] using 193 nm photolysis of 3-pentanone as precursor. Using the kinetic method, they determined $\sigma_{7596\text{ cm}^{-1}} = (3 \pm 1.5) \times 10^{-21} \text{ cm}^2$, which is 3 times smaller than the present value. A higher absorption cross section has also been measured previously by our group for the CH_3O_2 radical [13]. One possible reason might be that the determination from Atkinson and Spillman is based on the kinetic method using low initial radical concentrations, hence the $\text{C}_2\text{H}_5\text{O}_2$ concentration has to be measured over long reaction times in order to observe a sizeable decay, but the possible loss due to diffusion out of the photolysis volume or due to wall loss has not been considered in the data evaluation. This can induce an overestimation of the radical concentration and therefore an underestimation of the absorption cross section (see **Figure 2(c)** and **Figure 4**). Another reason might be the precursor: the reaction of $\text{C}_2\text{H}_5 + \text{O}_2$ can also lead to small amounts of HO_2 through (R7b), around 1% of the initial Cl-atom concentration led to formation of HO_2 in the experiments of this work. Atkinson and Spillman used 193 nm photolysis of 3-pentanone, which leaves considerably higher amounts of excess energy in the fragments than our method, based on H-atom abstraction. Therefore, the fraction of C_2H_5 radicals that react through (R6b) might be considerably higher than in our case. This could induce a non-negligible initial HO_2 concentration which participates in the removal of $\text{C}_2\text{H}_5\text{O}_2$ and would thus induce a systematic error when using the kinetic method. This is also in line with the observation of Atkinson and Spillman, that in their experiments the apparent rate constant of the $\text{C}_2\text{H}_5\text{O}_2$ self-reaction was inversely pressure dependant: the rate constant decreased with increasing pressure (D. Atkinson, private communication). An increased cooling of the hot C_2H_5 radical with increasing pressure would lead to a decreasing HO_2 concentration and thus to a slow-down of $\text{C}_2\text{H}_5\text{O}_2$ decay.

Rupper *et al.* [16] estimated the absolute absorption cross section to $\sigma = 4.4 \times 10^{-21} \text{ cm}^2$ from calculating the initial Cl-atom concentration by measuring the decrease of photolysis energy in absence and presence of the Cl-atom precursor, assuming that all generated Cl-atoms lead to formation of one $\text{C}_2\text{H}_5\text{O}_2$. In a more recent work from the same group, Melnik *et al.* [18] have determined the absorption cross section by dual-CRDS method: on one absorption path they measured the absorption of $\text{C}_2\text{H}_5\text{O}_2$ while on the other path the

concentration of HCl was quantified thanks to its known absorption cross section. Assuming again that one $\text{C}_2\text{H}_5\text{O}_2$ has been generated for each molecule of HCl, they found an absorption cross section of $\sigma = 5.29 \times 10^{-21} \text{ cm}^2$. This is nearly 2 times lower than the value obtained in this work. A possible explanation might be that Melnik *et al.* and Rupper *et al.* both consider the complete conversion of Cl-atoms into $\text{C}_2\text{H}_5\text{O}_2$ radicals: a simple model is presented by Melnik *et al.* [17] showing the complete conversion of Cl-atoms into $\text{C}_2\text{H}_5\text{O}_2$. However, the very fast reactions of Cl-atoms with $\text{C}_2\text{H}_5\text{O}_2$ ($k = 1.5 \times 10^{-10} \text{ cm}^3 \text{ molecule}^{-1} \text{ s}^{-1}$) [43] and C_2H_5 ($k = 3 \times 10^{-10} \text{ cm}^3 \text{ molecule}^{-1} \text{ s}^{-1}$) [44] are omitted in this model, even though these reactions are non-negligible under their conditions of very high initial Cl-atom concentrations, well above 10^{15} cm^{-3} , combined with relatively low C_2H_6 concentrations ($1 \times 10^{16} \text{ cm}^{-3}$). These reactions result in a $\text{C}_2\text{H}_5\text{O}_2$ concentration that might be well below the initial Cl-atom concentration, depending on the overall radical concentration as well as on the C_2H_6 concentration. **Figure 7** shows a simulation using the model from Melnik *et al.*, but completed by the two fast reactions. The left graph shows the result using initial concentrations such as given by Melnik *et al.* ($[\text{Cl}]_0 = 2 \times 10^{15} \text{ cm}^{-3}$ and $[\text{C}_2\text{H}_6]_0 = 1 \times 10^{16} \text{ cm}^{-3}$), the right graph shows the model result with typical conditions such as used in this work for the determination of the absorption cross section ($[\text{Cl}]_0 = 5 \times 10^{13} \text{ cm}^{-3}$ and $[\text{C}_2\text{H}_6]_0 = 3 \times 10^{16} \text{ cm}^{-3}$). Under the high Cl / low C_2H_6 conditions of Melnik *et al.*, only 63% of the Cl-atoms have been converted to $\text{C}_2\text{H}_5\text{O}_2$, while 28% of the Cl-atoms have reacted with $\text{C}_2\text{H}_5\text{O}_2$ and 8% have reacted with C_2H_5 . Under the low Cl / high C_2H_6 conditions (right graph), virtually all Cl-atoms have been converted to $\text{C}_2\text{H}_5\text{O}_2$, less than 1% of the Cl-atoms have reacted with either $\text{C}_2\text{H}_5\text{O}_2$ or C_2H_5 . From this model one can suspect that the absorption cross sections of Melnik *et al.* [17] and Rupper *et al.* [16] are strongly underestimated, and a correction of the Melnik *et al.* value, based on the more complete model, would lead to $\sigma = 8.8 \times 10^{-21} \text{ cm}^2$, which gets into good agreement with the value found in this work.

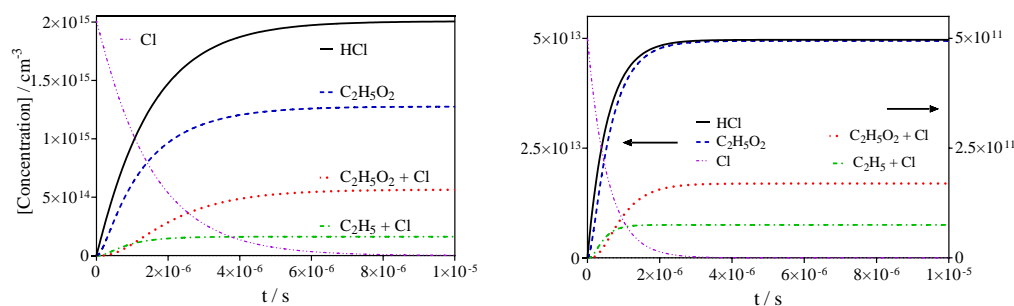


Figure 7: Simulation of conversion of Cl-atoms (violet dashed dot) into HCl (black) and $\text{C}_2\text{H}_5\text{O}_2$ (blue dashed): model taken from Melnik *et al.*, completed with the reactions of Cl with $\text{C}_2\text{H}_5\text{O}_2$ ($k = 1.5 \times 10^{-10} \text{ cm}^3 \text{ s}^{-1}$) [43] (red dotted) and C_2H_5 ($k = 3 \times 10^{-10} \text{ cm}^3 \text{ s}^{-1}$) [44] (green dashed dotted): left graph conditions such as used in Melnik *et al.* [17], right graph conditions such as used in this work. The products from the reaction of Cl with $\text{C}_2\text{H}_5\text{O}_2$ (red) and with C_2H_5 (green) are zoomed in the right graph by a factor of 100 (right y-axis applies)

5. Conclusions

We have presented in this work a new determination of the absorption cross section of the $\tilde{\text{A}} \leftarrow \tilde{\text{X}}$ electronic transition of the $\text{C}_2\text{H}_5\text{O}_2$ radical. The cross section at the peak wavelength 7596.4 cm^{-1} has in a first approach been determined by direct comparison with the well-known HO_2 absorption cross section in back-to-back experiments to be $(1.0 \pm 0.2) \times 10^{-20} \text{ cm}^2$. In further experiments, the absorption cross section has been validated by measuring the rate constant of $\text{C}_2\text{H}_5\text{O}_2$ with HO_2 in a wide range of concentration: the ratio of $[\text{HO}_2] / [\text{C}_2\text{H}_5\text{O}_2]$ has been varied between 0.2 and 3 and the concentration time profiles could be reproduced very well using the same absorption cross section for $\text{C}_2\text{H}_5\text{O}_2$, which returned a rate constant for the cross reaction of $6.5 \times 10^{-12} \text{ cm}^3 \text{ molecule}^{-1} \text{ s}^{-1}$. Sensitivity analysis in the upper and lower range of previous literature values did not allow anymore to

well reproduce the concentration-time profiles for both species over the entire concentration range and confirm the reliability of our results. Smaller absorption cross sections such as obtained in previous works can convincingly be explained by unidentified secondary reaction, not having been taken into account in the data evaluations.

Author Contributions: “Conceptualization, C.F.; methodology, C.F. C.Z., M.S., M.A.; validation, C.F., L.P., C.S.; formal analysis, C.Z., M.S.; investigation, C.Z., M.S., M.A.; resources, C.F., M.A.; data curation, C.F.; writing—original draft preparation, C.F.; writing—review and editing, all authors; visualization, C.Z., M.S., C.F.; supervision, C.F., L.P., X.T., W.Z.; project administration, C.F.; funding acquisition, C.F., L.P., C.S., X.T., W.Z.; All authors have read and agreed to the published version of the manuscript.”

Funding: This project was supported by the French ANR agency under contract No. ANR-11-Labx-0005-01 CaPPA (Chemical and Physical Properties of the Atmosphere), the Région Hauts-de-France, the Ministère de l'Enseignement Supérieur et de la Recherche (CPER Climibio) and the European Fund for Regional Economic Development. C.F. is grateful to the Chinese Academy of Sciences President's International Fellowship Initiative (No. 2018VMA0055). C.Z. thanks the Chinese Scholarship Council for financial support (No. 202006340125).

Data Availability Statement: Raw data are available on request.

Conflicts of Interest: The authors declare no conflict of interest.

References

1. Orlando, J.J.; Tyndall, G.S. Laboratory studies of organic peroxy radical chemistry: an overview with emphasis on recent issues of atmospheric significance. *Chem. Soc. Rev.* **2012**, *41*, 6294-6317, doi:10.1039/c2cs35166h.
2. Fittschen, C. The reaction of peroxy radicals with OH radicals. *Chem. Phys. Lett.* **2019**, *725*, 102-108, doi:10.1016/j.cplett.2019.04.002.
3. Assaf, E.; Song, B.; Tomas, A.; Schoemaeker, C.; Fittschen, C. Rate Constant of the Reaction between CH₃O₂ Radicals and OH Radicals revisited. *J. Phys. Chem. A* **2016**, *120*, 8923-8932, doi:10.1021/acs.jpca.6b07704.
4. Hasson, A.S.; Tyndall, G.S.; Orlando, J.J. A Product Yield Study of the Reaction of HO₂ Radicals with Ethyl Peroxy (C₂H₅O₂), Acetyl Peroxy (CH₃C(O)O₂), and Acetonyl Peroxy (CH₃C(O)CH₂O₂) Radicals. *J. Phys. Chem. A* **2004**, *108*, 5979-5989.
5. Tyndall, G.S.; Cox, R.A.; Granier, C.; Lesclaux, R.; Moortgat, G.K.; Pilling, M.J.; Ravishankara, A.R.; Wallington, T.J. Atmospheric Chemistry of Small Organic Peroxy Radicals. *J. Geophys. Res.* **2001**, *106*, 12157-12182.
6. Hunziker, H.E.; Wendt, H.R. Electronic Absorption Spectra of Organic Peroxyl Radicals in the Near Infrared. *J. Chem. Phys.* **1976**, *64*, 3488-3490.
7. Hunziker, H.E.; Wendt, H.R. Near infrared absorption spectrum of HO₂. *J. Chem. Phys.* **1974**, *60*, 4622-4623, doi:<http://doi.org/10.1063/1.1680949>.
8. O'Keefe, A.; Deacon, D.A.G. Cavity ring-down optical spectrometer for absorption measurements using pulsed laser sources. *Rev. Sci. Instrum.* **1988**, *59*, 2544-2551.
9. Romanini, D.; Kachanov, A.A.; Sadeghi, N.; Stoeckel, F. CW cavity ring down spectroscopy. *Chem. Phys. Lett.* **1997**, *264*, 316-322.
10. Pushkarsky, M.B.; Zalyubovsky, S.J.; Miller, T.A. Detection and Characterization of Alkyl Peroxy Radicals using Cavity Ringdown Spectroscopy. *J. Chem. Phys.* **2000**, *112*, 10695-10698.
11. Atkinson, D.B.; Spillman, J.L. Alkyl Peroxy Radical Kinetics Measured Using Near-infrared CW-Cavity Ring-down Spectroscopy. *J. Phys. Chem. A* **2002**, *106*, 8891-8902.
12. Thiebaud, J.; Crunaire, S.; Fittschen, C. Measurements of Line Strengths in the 2v₁ Band of the HO₂ Radical Using Laser Photolysis/Continuous Wave Cavity Ring-Down Spectroscopy (cw-CRDS). *The Journal of Physical Chemistry A* **2007**, *111*, 6959-6966, doi:10.1021/jp0703307.

13. Faragó, E.P.; Viskolcz, B.; Schoemaeker, C.; Fittschen, C. Absorption Spectrum and Absolute Absorption Cross Sections of CH_3O_2 Radicals and CH_3I Molecules in the Wavelength Range 7473–7497 cm^{-1} . *J. Phys. Chem. A* **2013**, *117*, 12802-12811, doi:10.1021/jp408686s.
14. Wen, Z.; Tang, X.; Fittschen, C.; Zhang, C.; Wang, T.; Wang, C.; Gu, X.; Zhang, W. Online analysis of gas-phase radical reactions using vacuum ultraviolet lamp photoionization and time-of-flight mass spectrometry. *Rev. Sci. Instrum.* **2020**, *91*, doi:10.1063/1.5135387.
15. Wen, Z.; Tang, X.; Wang, C.; Fittschen, C.; Wang, T.; Zhang, C.; Yang, J.; Pan, Y.; Liu, F.; Zhang, W. A vacuum ultraviolet photoionization time-of-flight mass spectrometer with high sensitivity for study of gas-phase radical reaction in a flow tube. *Int. J. Chem. Kinet.* **2019**, *51*, 178-188, doi:10.1002/kin.21241.
16. Rupper, P.; Sharp, E.N.; Tarczay, G.; Miller, T.A. Investigation of Ethyl Peroxy Radical Conformers via Cavity Ringdown Spectroscopy of the $\tilde{\text{A}}$ -X Electronic Transition. *J. Phys. Chem. A* **2007**, *111*, 832–840.
17. Melnik, D.; Chhantyal-Pun, R.; Miller, T.A. Measurements of the Absolute Absorption Cross Sections of the A-X Transition in Organic Peroxy Radicals by Dual-Wavelength Cavity Ring-Down Spectroscopy. *J. Phys. Chem. A* **2010**, *114*, 11583-11594.
18. Melnik, D.; Miller, T.A. Kinetic measurements of the $\text{C}_2\text{H}_5\text{O}_2$ radical using time-resolved cavity ring-down spectroscopy with a continuous source. *J. Chem. Phys.* **2013**, *139*, 094201.
19. Thiebaud, J.; Fittschen, C. Near Infrared cw-CRDS Coupled to Laser Photolysis: Spectroscopy and Kinetics of the HO_2 Radical. *Appl. Phys. B* **2006**, *85*, 383-389.
20. Parker, A.E.; Jain, C.; Schoemaeker, C.; Szriftgiser, P.; Votava, O.; Fittschen, C. Simultaneous, time-resolved measurements of OH and HO_2 radicals by coupling of high repetition rate LIF and cw-CRDS techniques to a laser photolysis reactor and its application to the photolysis of H_2O_2 . *Appl. Phys. B* **2011**, *103*, 725-733, doi:10.1007/s00340-010-4225-1.
21. Votava, O.; Mašát, M.; Parker, A.E.; Jain, C.; Fittschen, C. Microcontroller based resonance tracking unit for time resolved continuous wave cavity-ringdown spectroscopy measurements. *Rev. Sci. Instrum.* **2012**, *83*, 043110, doi:10.1063/1.3698061.
22. Assaf, E.; Asvany, O.; Votava, O.; Batut, S.; Schoemaeker, C.; Fittschen, C. Measurement of line strengths in the $\tilde{\text{A}}$ $2\text{A}' \leftarrow \text{X}$ $2\text{A}''$ transition of HO_2 and DO_2 . *J. Quant. Spectrosc. Radiat. Transfer* **2017**, *201*, 161-170, doi:<https://doi.org/10.1016/j.jqsrt.2017.07.004>.
23. Votava, O.; Masat, M.; Parker, A.E.; Jain, C.; Fittschen, C. Microcontroller Based Resonance Tracking unit for Time Resolved Continuous wave Cavity-Ringdown Spectroscopy Measurements. *Rev. Sci. Instrum.* **2012**, *83*, 043110.
24. Thiebaud, J.; Crunaire, S.; Fittschen, C. Measurement of Line Strengths in the $2\nu_1$ Band of the HO_2 Radical using Laser Photolysis / Continuous wave Cavity Ring Down Spectroscopy (cw-CRDS). *J. Phys. Chem. A* **2007**, *111*, 6959-6966.
25. Tang, Y.; Tyndall, G.S.; Orlando, J.J. Spectroscopic and Kinetic Properties of HO_2 Radicals and the Enhancement of the HO_2 Self Reaction by CH_3OH and H_2O . *J. Phys. Chem. A* **2010**, *114*, 369-378.
26. DeSain, J.D.; Ho, A.D.; Taatjes, C.A. High-resolution diode laser absorption spectroscopy of the O–H stretch overtone band (2,0,0)(0,0,0) of the HO_2 radical. *J. Mol. Spectrosc.* **2003**, *219*, 163-169.
27. Ibrahim, N.; Thiebaud, J.; Orphal, J.; Fittschen, C. Air-Broadening Coefficients of the HO_2 Radical in the $2\nu_1$ Band Measured Using cw-CRDS. *J. Mol. Spectrosc.* **2007**, *242*, 64-69.
28. Onel, L.; Brennan, A.; Gianella, M.; Ronnie, G.; Lawry Aguila, A.; Hancock, G.; Whalley, L.; Seakins, P.W.; Ritchie, G.A.D.; Heard, D.E. An intercomparison of HO_2 measurements by Fluorescence Assay by Gas Expansion and Cavity Ring-Down Spectroscopy within HIRAC (Highly Instrumented Reactor for Atmospheric Chemistry). *Atmos. Meas. Tech. Discuss.* **2017**, *10*, 4877-4894, doi:10.5194/amt-2017-268.
29. Assaf, E.; Liu, L.; Schoemaeker, C.; Fittschen, C. Absorption spectrum and absorption cross sections of the $2\nu_1$ band of HO_2 between 20 and 760 Torr air in the range 6636 and 6639 cm^{-1} . *Journal of Quantitative Spectroscopy & Radiative Transfer* **2018**, *211*, 107-114, doi:10.1016/j.jqsrt.2018.02.035.

-
30. Onel, L.; Brennan, A.; Gianella, M.; Ronnie, G.; Lawry Aguila, A.; Hancock, G.; Whalley, L.; Seakins, P.W.; Ritchie, G.A.D.; Heard, D.E. An intercomparison of HO₂ measurements by fluorescence assay by gas expansion and cavity ring-down spectroscopy within HIRAC (Highly Instrumented Reactor for Atmospheric Chemistry). *Atmos. Meas. Tech.* **2017**, *10*, 4877-4894, doi:10.5194/amt-10-4877-2017.
 31. Assali, M.; Rakovsky, J.; Votava, O.; Fittschen, C. Experimental Determination of the Rate Constants of the Reactions of HO₂ + DO₂ and DO₂ + DO₂. *Int. J. Chem. Kinet.* **2019**, Submitted.
 32. Atkinson, R.; Baulch, D.L.; Cox, R.A.; Crowley, J.N.; Hampson, R.F.; Hynes, R.G.; Jenkin, M.E.; Rossi, M.J.; Troe, J. Evaluated Kinetic and Photochemical Data for Atmospheric Chemistry: Volume 1 – Gas Phase Reactions of O_x, HO_x, NO_x, and SO_x Species, IUPAC Task Group on Atmospheric Chemical Kinetic Data Evaluation, <http://iupac.pole-ether.fr>." Vol 2. *Atmos. Chem. Phys.* **2004**, *4*, 1461-1738.
 33. Atkinson, R.; Baulch, D.L.; Cox, R.A.; Crowley, J.N.; Hampson, R.F.; Hynes, R.G.; Jenkin, M.E.; M. J. Rossi; Troe, J. Evaluated Kinetic and Photochemical Data for Atmospheric Chemistry: Volume II - Gas Phase Reactions of Organic Species. *Atmos. Chem. Phys.* **2006**, *6*, 3625-4055.
 34. Noell, A.C.; Alconcel, L.S.; Robichaud, D.J.; Okumura, M.; Sander, S.P. Near-Infrared Kinetic Spectroscopy of the HO₂ and C₂H₅O₂ Self-Reactions and Cross Reactions. *J. Phys. Chem. A* **2010**, *114*, 6983-6995.
 35. Boyd, A.A.; Flaud, P.-M.; Daugey, N.; Lesclaux, R. Rate Constants for RO₂ + HO₂ Reactions Measured under a Large Excess of HO₂. *J. Phys. Chem. A* **2003**, *107*, 818-821.
 36. Raventós-Duran, M.T.; Percival, C.J.; McGillen, M.R.; Hamer, P.D.; Shallcross, D.E. Kinetics and branching ratio studies of the reaction of C₂H₅O₂ + HO₂ using chemical ionisation mass spectrometry. *Phys. Chem. Chem. Phys.* **2007**, *9*, 4338 - 4348.
 37. Maricq, M.M.; Szente, J.J. A Kinetic Study of the Reaction between Ethylperoxy Radicals and HO₂. *J. Phys. Chem.* **1994**, *98*, 2078-2082.
 38. Fenter, F.F.; Catoire, V.; Lesclaux, R.; Lightfoot, P.D. The ethylperoxy radical: its ultraviolet spectrum, self-reaction, and reaction with hydroperoxy, each studied as a function of temperature. *J. Phys. Chem.* **1993**, *97*, 3530-3538.
 39. Dagaut, P.; Wallington, T.J.; Kurylo, M.J. Flash photolysis kinetic absorption spectroscopy study of the gasphase reaction HO₂ + C₂H₅O₂ over the temperature range 228 - 380K. *J. Phys. Chem.* **1988**, *92*, 3836-3839, doi:10.1021/j100324a031.
 40. Cattell, F.C.; Cavanagh, J.; Cox, R.A.; Jenkin, M.E. A kinetic study of reactions of HO₂ and C₂H₅O₂ using diode-laser absorption spectroscopy. *Journal of the Chemical Society-Faraday Transactions II* **1986**, *82*, 1999-2018, doi:10.1039/f29868201999.
 41. Fittschen, C.; Frenzel, A.; Imrik, K.; Devolder, P. Rate Constants for the Reactions of C₂H₅O, i-C₃H₇O, and n-C₃H₇O with NO and O₂ as a Function of Temperature. *Int. J. Chem. Kinet.* **1999**, *31*, 860-866.
 42. Fernandes, R.X.; Luther, K.; Marowsky, G.; Rissanen, M.P.; Timonen, R.; Troe, J. Experimental and Modeling Study of the Temperature and Pressure Dependence of the Reaction C₂H₅ + O₂ (+ M) → C₂H₅O₂ (+ M). *J. Phys. Chem. A* **2015**, *119*, 7263-7269, doi:10.1021/jp511672v.
 43. Maricq, M.M.; Szente, J.J.; Kaiser, E.W.; Shi, J. Reaction of Chlorine Atoms with Methylperoxy and Ethylperoxy Radicals. *J. Phys. Chem.* **1994**, *98*, 2083-2089, doi:10.1021/j100059a017.
 44. Seakins, P.W.; Woodbridge, E.L.; Leone, S.R. A laser flash photolysis, time-resolved Fourier Transform Infrared Emission study of the reaction Cl + C₂H₅ → HCl + C₂H₄. *J. Phys. Chem.* **1993**, *97*, 5633-5642, doi:10.1021/j100123a029.